Electronic Supplementary Material (ESI) for Nanoscale.

Supplementary information

Confined interfacial micelle aggregating assembly of ordered macro-mesoporous tungsten oxides for H_2S sensing

Tao Zhao,[a] Yuchi Fan,[a] Ziqi Sun,[b] Jianping Yang,[a] Xiaohang Zhu,[a] Wan Jiang,[a] Lianjun Wang,[a] Yonghui Deng,[c] Xiaowei Cheng,[c] Pengpeng Qiu*[a] and Wei Luo*[a]

[a] State Key Laboratory for Modification of Chemical Fibers and Polymer Materials, College of Materials Science and Engineering, Institute of Functional Materials, Donghua University, Shanghai 201620, China.
[b] School of Chemistry and Physics, Queensland University of Technology, Brisbane, Queensland 4000, Australia.
c Department of Chemistry, State Key Laboratory of Molecular Engineering of Polymers, Shanghai Key Laboratory of Molecular Catalysis and Innovative Materials, iChEM, Fudan University, Shanghai 200433, China

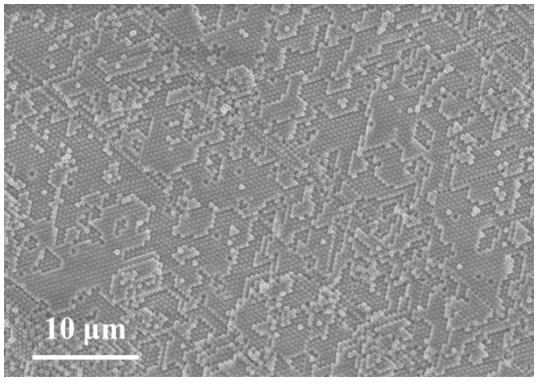

Fig. S1 SEM image of SiO_2 photonic crystals (PCs).

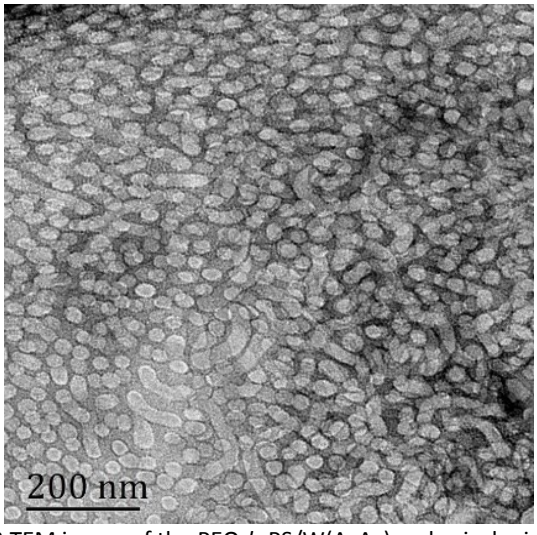

Fig. S2 TEM image of the PEO-*b*-PS/$W(AcAc)_6$ spherical micelles.

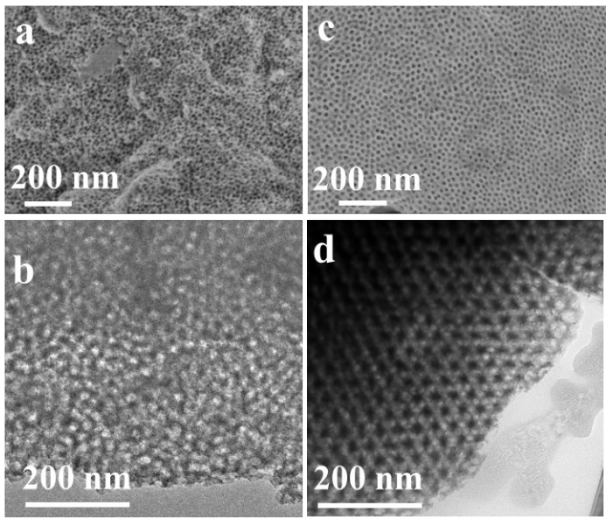

Fig. S3 SEM (a, c) and TEM (b, d) images of the structure and morphology of the tungsten oxide as a function of reaction time, 60 min (a, b) and 120 min (c, d).

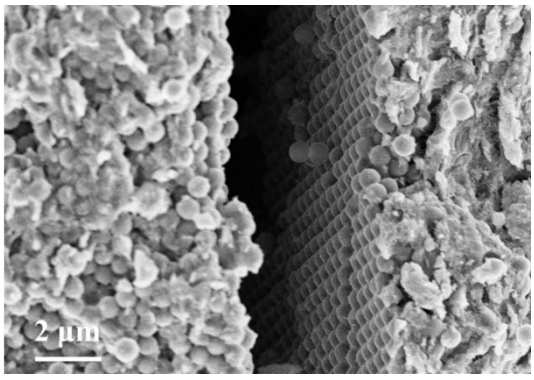

Fig. S4 SEM image of SiO_2 PCs/WO_3 composites

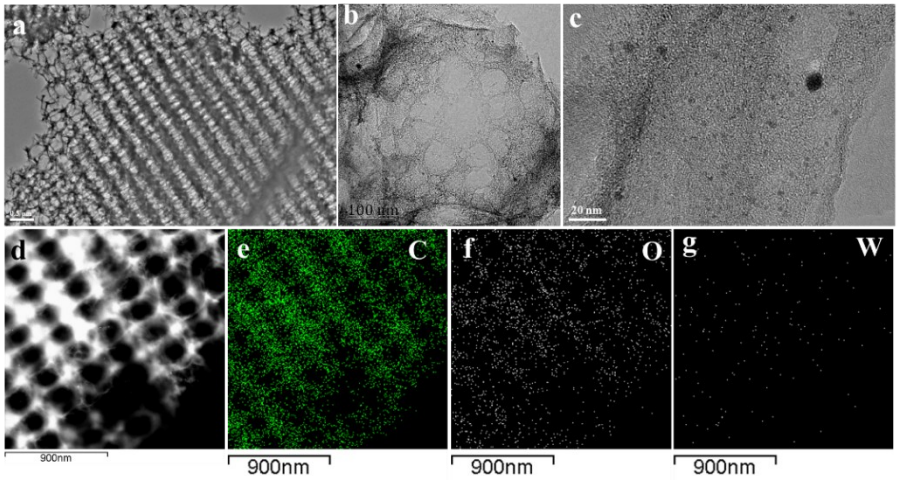

Fig. S5 TEM images (a-c) of the ordered macro/mesoporous carbon after etching out SiO_2 and WO_3, STEM image (d) and corresponding element distribution (e-g).

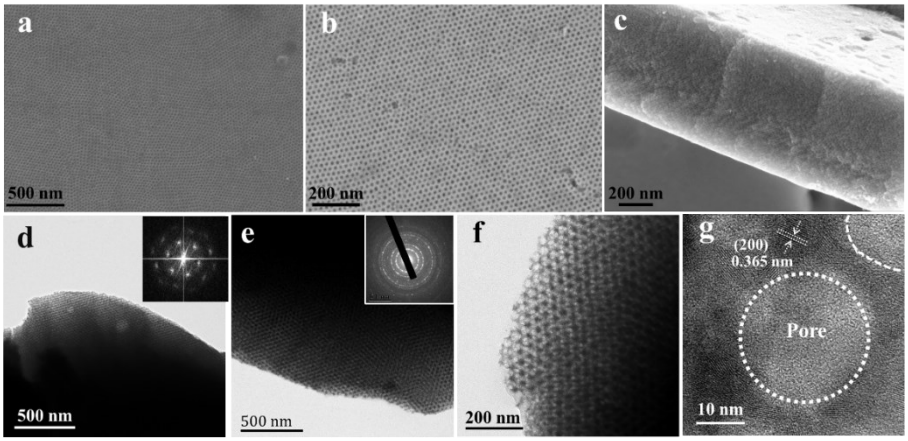

Fig. S6 SEM (a-c), TEM (d-f) taken along at different facets [110] (d), [211] (e) and [111] (f), and HRTEM (g) images of mesoporous WO_3. The insets in d and e are the corresponded fast Fourier transform and selected area electron diffraction, respectively.

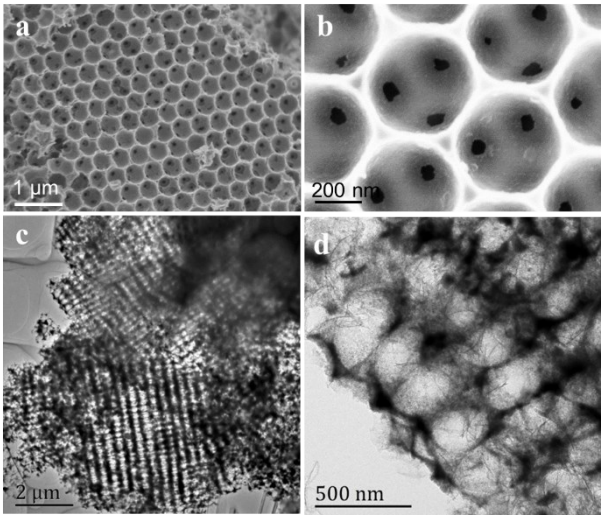

Fig. S7 SEM (a, b) and TEM (c, d) images of macroporous WO_3.

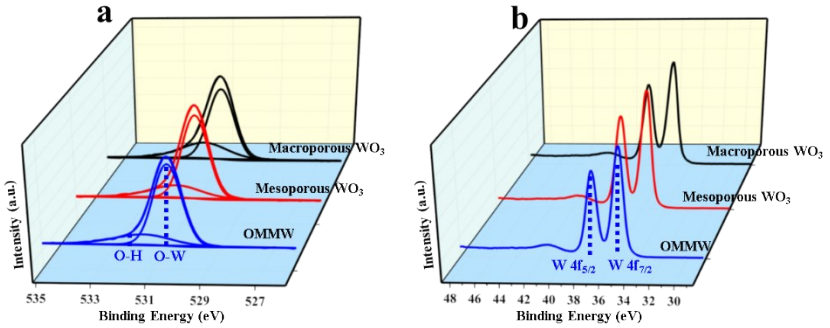

Fig. S8 XPS core-level spectra of O 1s (a) and W 4f (b) for porous WO_3 materials.

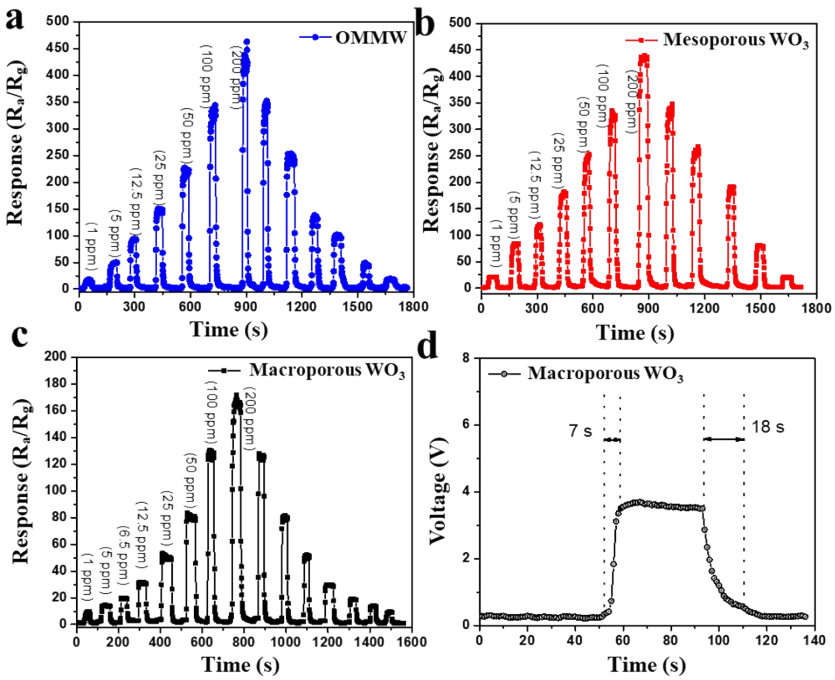

Fig. S9. Response–recovery curve of OMMW (a), mesoporous WO_3 sensor (b) and macroporous WO_3 sensor (c) toward H_2S with different concentrations and dynamic response–recovery curve of macroporous WO_3 (c) toward 50 ppm of H_2S.

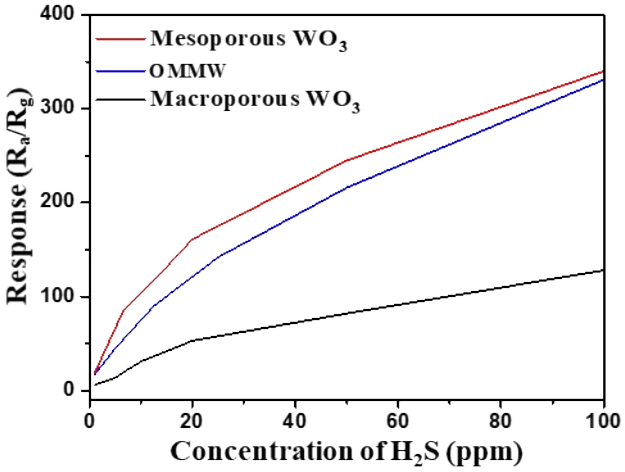

Fig. S10. Response of the sensors toward different H_2S concentration based on the three WO_3-based sensor (c)

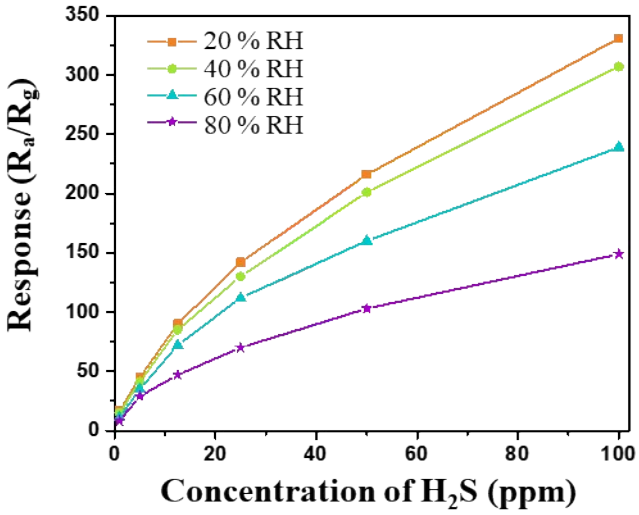

Fig. S11. Responses of OMMW to 1–100 ppm H_2S at different relative humidity.

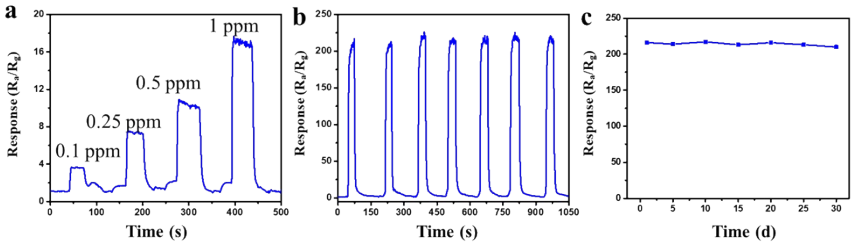

Fig. S12 Response–recovery curve of ordered macro-mesoporous WO_3 nanostructures toward H_2S with an ultralow concentration (a), response and recovery curve of OMMW toward 50 ppm of H_2S for seven cycles (b), and stability test toward 50 ppm of H_2S for 30 days (c).

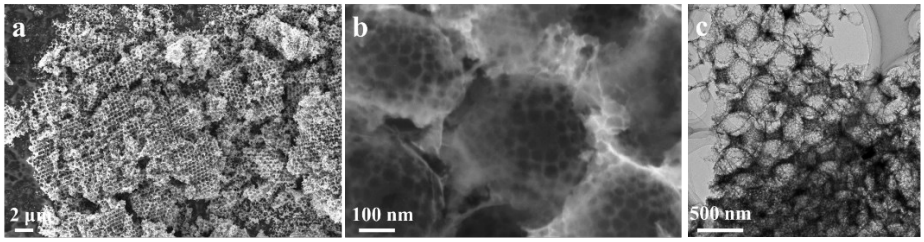

Fig. S13 SEM and TEM image of OMMW after the cycle gas sensing test

Table S1 Physical properties of WO_3.

Materials	Surface area ($m^2\ g^{-1}$)	Pore size (nm)	Pore volume ($cm^3\ g^{-1}$)
OMMW	78	34.1	0.24
Mesoporous WO_3	98	19.4	0.13
Macroporous WO_3	35	59.2	0.08

Table S2. Comparison of H_2S sensing performances

Materials and morphology	Concentration (H_2S)	Sensitivity (Ra/Rg)	Response/recovery time(s)	Detection limit	Ref
SnO2/rGO/PANI	5 ppm	4.3	121/117	0.05	[4]
Porous ZnO hollow tubule	100 ppb	2<	>29/>98	10 ppb	[47]
Fe_2O_3 nanoboxes	5 ppm	6	31/187	0.25	[48]
Flower-like WO_3	20 ppm	10.9	0.9/19	0.3	[16]
Mesoporous WO_3	50	262	2/38	0.25	[30]
WO_3 nanotube	5 ppm	11.45	>10/>120	0.03	[49]
WO_3 microbelts	5 ppm	11.7	8/260	0.4	[50]
V_2O_5-WO_3	60 ppm	22.3	155/148	5 ppm	[51]
Flower-like WO_3/CuO	5 ppm	105	42/10	0.25	[52]
Net-like SnO_2/ZnO	5 ppm	112	>500/>40s	0.1ppm	[53]
Macroporous WO_3	50 ppm	82	7/18	0.25 ppm	This work
OMMW	50 ppm	216	4/20 (s)	0.25 ppm	This work